ELSEVIER

J. Non-Newtonian Fluid Mech., 78 (1998) 91–118

Journal of Non-Newtonian Fluid Mechanics

A finite volume approach in the simulation of viscoelastic expansion flows

K.A. Missirlis [a], D. Assimacopoulos [a], E. Mitsoulis [b,*]

[a] *Department of Chemical Engineering, National Technical University of Athens, Athens 157-80, Greece*
[b] *Department of Mining Engineering and Metallurgy, National Technical University of Athens, Athens 157-80, Greece*

Received 17 March 1997; received in revised form 10 December 1997

Abstract

A finite volume technique is presented for the numerical solution of viscoelastic flows. The flow of a differential upper-convected Maxwell (UCM) model fluid through an abrupt expansion has been chosen as a prototype example due to the existence of previous simulations in the literature. The conservation and constitutive equations are solved using the finite volume method (FVM) in a non-staggered grid with an upwind scheme for the viscoelastic stresses and a hybrid scheme for the velocities. An enhanced-in-speed pressure-correction algorithm is used and a new method for handling the source term of the momentum equations is introduced. Improved accuracy is achieved by a special discretization of the boundary conditions. Stable solutions are found for high Deborah numbers, further extending the range of previous similar simulations with the FVM. The solutions have been verified with grid refinement and show that at high elasticity levels, the domain length must be long enough to accommodate the slow relaxation of high viscoelastic stresses. The FVM is proven quite capable for numerically handling viscoelastic models with low computational cost and its use is recommended as a viable alternative to the solution of viscoelastic problems using a variety of constitutive models.

Keywords: Expansion flows; UCM constitutive equation; Viscoelasticity; Upwinding; Finite-volume method; Non-staggered grid

1. Introduction

In the continuing effort to handle viscoelasticity through constitutive modelling and numerical simulations, considerable effort has been expended for this dual task in the last 15–20 years. Remarkable progress has been achieved in both aspects. From the modelling point of view, a variety of constitutive models have been used, both of the differential and of the integral type [1,2]. Regarding the former type, most of the efforts have been dedicated to the solution of the

* Corresponding author. Fax: + 301 7722173; e-mail: mitsouli@metal.ntua.gr

0377-0257/98/$19.00
PII S0377-0257(98)00057-3

upper-convected Maxwell (UCM) fluid model, the Oldroyd-B, Phan-Thien/Tanner, Giesekus, Leonov, etc. models. Regarding the latter type, the major emphasis has been on the K-BKZ integral model and its variants, the Wagner model and the PSM model [3]. The current state of affairs has shown that it is possible to model adequately polymer solution and polymer melt behaviour by employing multi-mode models with a spectrum of relaxation times, either of the differential or the integral type, with equivalent results [4,5]. Thus, the modelling efforts are still very active and have shown steady progress, especially in well-defined flows with absence or presence of singularities.

From the numerical point of view, many numerical methods have been used and a variety of results have been produced. Early attempts were based on the finite difference method (FDM) [6–8]. The majority of the simulations have been carried out with the FEM [9]. A serious attempt originated with Tanner's group, using the BEM [10,11]. Good results have also been obtained by using spectral finite element methods (S-FEM) [12]. While each one of them has its advantages and disadvantages, the search for even better and/or faster methods still continues. In that respect, it was inevitable that the finite volume method (FVM) would also be tried within the viscoelastic context, since this method is well-known and has been widely used with success in other fields of computational fluid mechanics [13]. However, the viscoelastic simulations with the FVM are very limited [14–17]. Quite recently, renewed interest has surfaced, notably by the Phan-Thien/Tanner group [18–20] and by Luo [21].

In forming methods, e.g. extrusion and injection moulding, various polymers are shaped by passing through a channel with an abrupt change of geometry. Several numerical studies have focused on the viscoelastic flow through a sudden contraction or expansion. One of the difficulties in the simulation of these flows is the severe change of geometry along the channel. This causes very high stress levels, which enhance numerical instability. Early calculations [6,7] were plagued by loss of convergence for relatively low values of the dimensionless Deborah number ($De < 0.3$). Numerical difficulties arising by the presence of corners have been addressed by Keunings [1].

A simple model, but very difficult to solve in the presence of a corner, is the UCM model. The unknown complex flow near the singularity results in early loss of convergence when the grid density or the fluid elasticity become substantial. The elasticity of the fluid expressed by De poses an upper limit beyond which loss of convergence occurs. A previous study on viscoelastic flow in an abrupt axisymmetric contraction using FVM was performed by Sasmal [17]. His results are smooth and convergent for De up to 6.25, but for De over 1.5 the results are highly grid-dependent. Simulations for the UCM fluid in expansion channels have not received much attention in the literature. Recently, Darwish et al. [16] studied this geometry, but the grid density was confined only to 336 cells within a short domain and the results for all primitive variables are presented for De equal to 1.2 (or their corresponding Weissenberg number, We), while for De equal to 2.4 only the velocity and pressure fields are presented as well as the streamlines and they show unrealistic variation.

In this paper, we re-examine the flow of a UCM model fluid through a 4:1 sudden planar expansion using a stable finite volume scheme. The solution method succeeds to provide accurate numerical solutions in agreement with the analytical solutions in the fully-developed regions of the flow field, for elasticity levels up to $De = 3.0$ with a variety of grids to establish results independent of grid density.

In the following sections, the description of the problem, the mathematical modelling of the flow and the solution method are cited. The discretization of the source term and the boundary conditions are separately examined. Finally, the results of the numerical simulations are presented and conclusions are drawn regarding the use of FVM for viscoelastic flow simulations.

2. Mathematical modelling

2.1. Conservation and constitutive equations—dimensionless parameters

The problem geometry is shown in Fig. 1. It concerns the flow of a UCM fluid through a planar 4:1 sudden expansion. The channel has an upstream length of $L = 4H$ and a downstream length equal to $L_{res} = 10H$ (to match earlier simulations by Darwish et al. [16]) or $30H$ for flows with higher elasticity levels.

The isothermal flow through expansions and contractions for incompressible fluids, such as polymer solutions and melts, is governed by the usual conservation equations of mass and momentum, i.e.

$$\nabla \cdot \boldsymbol{v} = 0, \tag{1}$$

$$\rho \boldsymbol{v} \cdot \nabla \boldsymbol{v} = -\nabla P + \nabla \cdot \boldsymbol{\tau}, \tag{2}$$

where $\boldsymbol{v}$ is the velocity vector, P is the scalar pressure, τ is the extra stress tensor and ρ is the density. In Eq. (2), the inertia term has been included.

The constitutive equation that relates the stresses $\boldsymbol{\tau}$ to the deformation history is the UCM model, which in its differential form is written as [22]

$$\boldsymbol{\tau} + \lambda \overset{\nabla}{\boldsymbol{\tau}} = \mu \dot{\gamma}, \tag{3}$$

where λ is a constant relaxation time, μ is a constant viscosity and $\dot{\gamma}$ is the rate-of-strain tensor given by

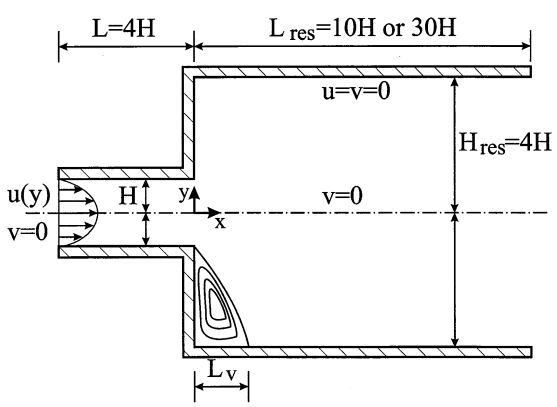

Fig. 1. Schematic representation of the planar sudden expansion with notation and boundary conditions.

$$\dot{\gamma} = \boldsymbol{L}^{\mathrm{T}} + \boldsymbol{L}, \tag{4}$$

where $\boldsymbol{L}$ is the velocity gradient tensor given by

$$\boldsymbol{L} = \nabla \boldsymbol{v}^{\mathrm{T}}, \tag{5}$$

with T denoting the transpose operation. The symbol over the stress tensor in Eq. (3) denotes the upper-convected derivative, i.e.

$$\overset{\nabla}{\boldsymbol{\tau}} = \frac{\partial \boldsymbol{\tau}}{\partial t} + \boldsymbol{v} \cdot \nabla \boldsymbol{\tau} - \boldsymbol{L} \cdot \tau - \boldsymbol{\tau} \cdot \boldsymbol{L}^{\mathrm{T}}. \tag{6}$$

For a two-dimensional system of rectangular co-ordinates (x, y) with velocity components (u, v), the conservation equation for continuity (1) can be written as

$$\frac{\partial u}{\partial x} + \frac{\partial v}{\partial y} = 0, \tag{7}$$

the momentum Eq. (2) is given by

$$\frac{\partial}{\partial x}(\rho uu) + \frac{\partial}{\partial y}(\rho uv) = \frac{\partial \boldsymbol{\tau}_{xx}}{\partial x} + \frac{\partial \boldsymbol{\tau}_{xy}}{\partial y} - \frac{\partial P}{\partial x}, \tag{8}$$

$$\frac{\partial}{\partial x}(\rho vv) + \frac{\partial}{\partial y}(\rho vu) = \frac{\partial \boldsymbol{\tau}_{yy}}{\partial y} + \frac{\partial \boldsymbol{\tau}_{xy}}{\partial x} - \frac{\partial P}{\partial y}, \tag{9}$$

and the constitutive equations for the UCM model can be written as

$$\frac{\partial}{\partial x}(\lambda u \boldsymbol{\tau}_{xx}) + \frac{\partial}{\partial y}(\lambda v \boldsymbol{\tau}_{xx}) = 2\mu \frac{\partial u}{\partial x} - \left(1 - 2\lambda \frac{\partial u}{\partial x}\right)\boldsymbol{\tau}_{xx} + 2\lambda \frac{\partial u}{\partial y}\boldsymbol{\tau}_{xy}, \tag{10}$$

$$\frac{\partial}{\partial x}(\lambda u \boldsymbol{\tau}_{yy}) + \frac{\partial}{\partial y}(\lambda v \boldsymbol{\tau}_{yy}) = 2\mu \frac{\partial v}{\partial y} - \left(1 - 2\lambda \frac{\partial v}{\partial y}\right)\boldsymbol{\tau}_{yy} + 2\lambda \frac{\partial v}{\partial x}\boldsymbol{\tau}_{xy}, \tag{11}$$

$$\frac{\partial}{\partial x}(\lambda u \boldsymbol{\tau}_{xy}) + \frac{\partial}{\partial y}(\lambda v \boldsymbol{\tau}_{xy}) = \mu\left(\frac{\partial v}{\partial x} + \frac{\partial u}{\partial y}\right) - \boldsymbol{\tau}_{xy} + \lambda \frac{\partial v}{\partial x}\boldsymbol{\tau}_{xx} + \lambda \frac{\partial u}{\partial y}\boldsymbol{\tau}_{yy}. \tag{12}$$

For the flow boundary conditions and referring to Fig. 1, we have the usual no-slip boundary condition on the walls for the velocities, fully-developed profiles upstream at the channel entrance, while at the centerline we have zero axial velocity. At the exit, the mass balance for the fluid is satisfied.

The dimensionless parameters often used to describe isothermal viscoelastic flows with inertia are the Deborah number (De) and the Reynolds number (Re) defined by [22]

$$\mathrm{De} = \lambda \dot{\gamma} = \lambda \frac{U}{H}, \tag{13}$$

$$\mathrm{Re} = \frac{\rho U H}{\mu}, \tag{14}$$

where $\dot{\gamma}$ is a nominal shear rate (usually taken as the wall shear rate in fully-developed flow), U is a characteristic velocity and H is a characteristic length. It is seen that for a given fluid with

Table 1
The terms in the conservation equations for a two-dimensional flow

Equation	φ	Γ	S
Continuity	1	0	0
u-Momentum	u	μ	$-\frac{\partial P}{\partial x}+\frac{\partial}{\partial x}\left(\tau_{xx}-2\mu\frac{\partial u}{\partial x}\right)+\frac{\partial}{\partial y}\left[\tau_{xy}-\mu\left(\frac{\partial u}{\partial y}+\frac{\partial v}{\partial x}\right)\right]$
v-Momentum	v	μ	$-\frac{\partial P}{\partial y}+\frac{\partial}{\partial y}\left(\tau_{yy}-2\mu\frac{\partial v}{\partial y}\right)+\frac{\partial}{\partial x}\left[\tau_{xy}-\mu\left(\frac{\partial u}{\partial y}+\frac{\partial v}{\partial x}\right)\right]$
Normal stress τ_{xx}	τ_{xx}	0	$2\mu\frac{\partial u}{\partial x}-\left(1-2\lambda\frac{\partial u}{\partial x}\right)\tau_{xx}+2\lambda\frac{\partial u}{\partial y}\tau_{xy}$
Normal stress τ_{yy}	τ_{yy}	0	$2\mu\frac{\partial v}{\partial y}-\left(1-2\lambda\frac{\partial v}{\partial y}\right)\tau_{yy}+2\lambda\frac{\partial v}{\partial x}\tau_{xy}$
Shear stress τ_{xy}	τ_{xy}	0	$\mu\left(\frac{\partial u}{\partial y}+\frac{\partial v}{\partial x}\right)-\tau_{xy}+\lambda\frac{\partial v}{\partial x}\tau_{xx}+\lambda\frac{\partial u}{\partial y}\tau_{yy}$

constant material properties λ, μ and ρ, both De and Re show a linear increase with average velocity U or flow rate.

In the present simulations, we take U as the average inlet velocity and H as the half channel height (Fig. 1) and increase the Deborah number by increasing the relaxation time. Note that in the work of Darwish et al. [16], in their definition of the Weissenberg number (We), H is also taken as half the channel height and thus, We = De.

3. Method of solution

The constitutive Eq. (3) is solved together with the conservation Eqs. (1) and (2) using the FVM. Previous work with the FVM on viscoelastic flows is recorded by various research groups in their papers [14–21]. Here we give some details about our own implementation of the method.

3.1. Numerical method

When employing the FVM, the governing equations are written in the following general form [13]:

$$\nabla\cdot(m\boldsymbol{v}\varphi)=\nabla\cdot(\Gamma\nabla\varphi)+S, \tag{15}$$

where m is either the density ρ or relaxation time λ, depending on the conservation or constitutive equation, φ is the primitive variable, Γ is the diffusion coefficient and S is the source term. For the form of primitive variable φ, diffusion coefficient Γ and source term S for each equation, refer to Table 1.

The flow domain is divided into a number of control volumes over which Eq. (15) is integrated. The information needed for the computation of variable φ is its variation between consecutive control volumes (the variable φ is affected only by the value of φ at neighbouring control volumes). The control volume (cell) is the basic element of the discretization method. The boundaries of the

cells are determined first and then grid points are placed at their center. The computational points on the boundaries belong to control volumes reduced by one dimension (or by two dimensions if they are at the corners of the computational domain). In this way there are no special discretization equations for the boundaries or the boundary conditions.

The differential Eq. (15) to be numerically solved must be first integrated over the cell. The residuals of the integration of Eq. (2) are used to control convergence during the solution process. For each primitive variable a different residual is calculated. When all the residuals are smaller than a predetermined set of values, then the solution has converged.

Each control volume has magnitude $V = \Delta x \times \Delta y \times R$ (in the case of rectangular coordinates, the radius R is equal to unity). Integrating Eq. (15) over the control volume as shown in Fig. 2 yields

$$\int_V \mathrm{div}(\rho \boldsymbol{u}\varphi)\,\mathrm{d}V = \int_V \mathrm{div}(\Gamma\ \mathrm{grad}\ \varphi)\,\mathrm{d}V + \int_V S\,\mathrm{d}V, \tag{16}$$

and converting to surface integrals in Eq. (16) according to the divergence theorem yields:

$$\oiint_A (\rho v\varphi)\cdot \underline{n}\,\mathrm{d}A = \oiint_A (\Gamma\nabla\varphi)\cdot \underline{n}\,\mathrm{d}A + \int_V S\,\mathrm{d}V \tag{17}$$

where A is the surface around volume V and $\underline{n}$ the unit vector normal to the surface.

The term S is generally assumed to be a linear function of variable ϕ:

$$S = S_C + S_P\varphi_P. \tag{18}$$

The integrals in Eq. (17) are calculated according to the following assumptions:

- the values of properties at the center of a control volume are equal to those prevailing on the entire control volume and
- the values of properties at the center of the surface of a control volume are equal to those prevailing on the entire surface,

so Eq. (17) can be written as

$$\int_s^n \int_w^e (\rho \boldsymbol{v}\varphi)\,\mathrm{d}x\,\mathrm{d}y = \int_s^n \int_w^e \Gamma\left(\frac{\partial\varphi}{\partial x} + \frac{\partial\varphi}{\partial y}\right)\mathrm{d}x\,\mathrm{d}y + (S_C + S_P\varphi_P)V \tag{19}$$

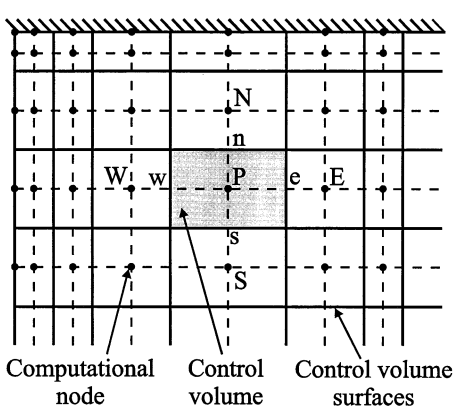

Fig. 2. Grid distribution for the computational domain.

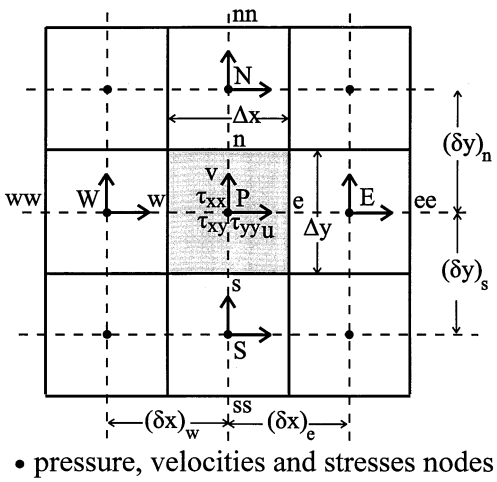

Fig. 3. Control volume centred around node P for a two-dimensional non-staggered grid along with computational variables.

or

$$\left[(\rho u\varphi)_e - \Gamma_e\left(\frac{\partial\varphi}{\partial x}\right)_e\right]A_e - \left[(\rho u\varphi)_w - \Gamma_w\left(\frac{\partial\varphi}{\partial x}\right)_w\right]A_w + \left[(\rho u\varphi)_n - \Gamma_n\left(\frac{\partial\varphi}{\partial x}\right)_n\right]A_n - \left[(\rho u\varphi)_s - \Gamma_s\left(\frac{\partial\varphi}{\partial x}\right)_s\right]A_s = (S_C + S_P\varphi_P)V, \tag{20}$$

and in pseudo-linear form as

$$\alpha_P\varphi_P = \sum_I \alpha_1\varphi_1 + b, \tag{21}$$

where the index $I\in\{E, W, N, S\}$ denotes summation over all the neighbouring to P nodes.

The terms in Eq. (21) have the following form:

$$a_P = \sum_I a_I - S_P\,\Delta x\,\Delta y, \tag{22}$$

$$a_I = D_i A(|\mathrm{Pe}_i|) + \max(F_i, 0), \tag{23}$$

$$b = S_C\,\Delta x\,\Delta y, \tag{24}$$

where Pe_i is the local Peclet number defined by $\mathrm{Pe}_i = F_i/D_i$, while $A(|\mathrm{Pe}_i|)$, $i\in\{e, w, n, s\}$ is a function of the discretization scheme, F_i are the mass outflow rates through the corresponding cell surface and D_i are the diffusion terms. Note that the index I refers to the computational nodes, while the index i refers to the control volume surfaces (Figs. 2 and 3).

For an upwind scheme used in the constitutive equations for the stresses:

$$A(|\mathrm{Pe}_i|) = 1, \tag{25}$$

while for a hybrid scheme used in the momentum equations:

$$A(|\mathrm{Pe}_i|) = \max(0, 1 - 0.5|\mathrm{Pe}_i|) \tag{26}$$

A problem arises for the pressure computation in the source term of the momentum equations, because there is no special conservation equation for pressure. The pressure has correct values only when the continuity equation is satisfied for the velocity values derived from the momentum equations. The term ∇P in the momentum equation is integrated over each control volume. The discretization equation, e.g. for the horizontal direction (Fig. 3), contains the term $P_w - P_e$, which is the net force per surface unit applied to the control volume. The above term has the following form:

$$P_w - P_e = [f_W^x P_P + (1 - f_W^x) P_W] - [f_P^x P_E + (1 - f_P^x) P_P], \tag{27}$$

where f_W^x, f_P^x are the coefficients of linear interpolation for the east face of nodes W and P, respectively [13].

The coefficients of linear interpolation are used to calculate the primitive variable on the face between two nodes. For a uniform grid where $f_W^x = f_P^x = 0.5$, the computed pressure values are derived from two non-neighbouring cells, i.e. from a grid having half the density of the initial one; the result is a reduced accuracy. In an even worse case, where an alternating pressure field exists, the pressure difference $P_w - P_e$ for each cell can be equal to zero and a uniform pressure field is produced. The above difficulty is resolved, as Patankar [13] states, using a different grid (staggered) for all primitive variables except pressure. In such a grid, the velocities and stresses are computed and stored at different locations than the pressure. Of course, this technique increases the complexity of the solution procedure.

In this work the primitive variables are stored on the same grid points and the resulting grid arrangement is called non-staggered (Fig. 3). The advantage of a non-staggered grid is its simplicity with regard to the geometry variables in the conservation equations [23,24].

To overcome the pressure computation problem in non-staggered grids, different methods are used to compute the pressure at the surfaces of the control volumes. In the present paper, the momentum interpolation method is used [24] (Appendix A). The computation of velocities at the control volume surfaces is performed using a combination of the discretized equations for two neighbouring cells. In the momentum equations, the variables which refer to the control volume surfaces are computed by linear interpolation of the neighbouring values of the same variable. This applies to all primitive variables except pressure [24].

3.2. Solution algorithm

Many algorithms have been developed over the years to calculate the pressure field. The first widely used method was the semi-implicit method for the pressure-linked equation (SIMPLE) [13]. Many modifications of the SIMPLE method have also been proposed, such as SIMPLE revised (SIMPLER) [13] and the SIMPLE consistent (SIMPLEC) algorithm of Van Doormal and Raithby [25]. However, these algorithms require extensions in order to handle viscoelasticity. Thus, an alternative algorithm named pressure implicit momentum explicit (PRIME) was introduced by Maliska and Raithby [26]. A modified PRIME algorithm was used by Darwish et al. [16], but was found to be too time-consuming.

In the present paper, a new algorithm to handle the UCM model is proposed. In this algorithm the conservation equations for the stresses are written in terms of total stress applied to a control volume, although other groups [17,19] write the conservation equations for the stresses in terms of the extra stress tensor. Using the current formulation the computation of stresses is much simplified. The steps of the present algorithm are as follows:

- Computation of stresses.
- Computation of extra stress gradients (explained in the next section).
- Special handling of source terms in the momentum equations (explained in the next section).
- Computation of velocities.
- Computation of pressure and correction of velocities.
- Convergence control and return to first step if necessary.

This algorithm is faster than the modified PRIME algorithm used by Darwish et al. [16], where the pressure and stress fields were calculated twice for each iteration. With this algorithm the total stress field is obtained directly, avoiding extra calculations spent on the addition of viscous and extra stresses. The pressure and stress fields are calculated only once for each iteration.

3.3. Discretization of momentum equations

Eqs. (8) and (9) can be written in the general form of Eq. (15) using the following transformation, [7]:

$$\tau'_{xx} = \tau_{xx} - 2\mu \frac{\partial u}{\partial x}, \tag{28}$$

$$\tau'_{yy} = \tau_{yy} - 2\mu \frac{\partial v}{\partial y}, \tag{29}$$

$$\tau'_{xy} = \tau_{xy} - \mu\left(\frac{\partial u}{\partial y} + \frac{\partial v}{\partial x}\right), \tag{30}$$

where τ' is the elastic part of the stress tensor τ.

Substituting Eqs. (28)–(30) in the momentum equations and assuming constant viscosity, Eqs. (8) and (9) can be written

$$\frac{\partial}{\partial x}(\rho uu) + \frac{\partial}{\partial y}(\rho uv) = \underbrace{\mu \frac{\partial}{\partial x}\left(\frac{\partial u}{\partial x}\right) + \mu \frac{\partial}{\partial y}\left(\frac{\partial u}{\partial y}\right)}_{} + \underbrace{\frac{\partial \tau'_{xx}}{\partial x} + \frac{\partial \tau'_{xy}}{\partial y}}_{} + \mu \frac{\partial}{\partial x}\left(\frac{\partial u}{\partial x} + \frac{\partial v}{\partial y}\right) - \frac{\partial P}{\partial x}, \tag{31}$$

$$\frac{\partial}{\partial x}(\rho vv) + \frac{\partial}{\partial y}(\rho vu) = \underbrace{\mu \frac{\partial}{\partial x}\left(\frac{\partial v}{\partial x}\right) + \mu \frac{\partial}{\partial y}\left(\frac{\partial v}{\partial y}\right)}_{} + \underbrace{\frac{\partial \tau'_{yy}}{\partial y} + \frac{\partial \tau'_{xy}}{\partial x}}_{} + \mu \frac{\partial}{\partial y}\left(\frac{\partial u}{\partial x} + \frac{\partial v}{\partial y}\right) - \frac{\partial P}{\partial y} \tag{32}$$

In Eqs. (31) and (32) the viscous parts are discretized as the diffusion terms of the general Eq. (15)[13], while the other terms on the right-hand side are treated as extra source terms.

The proper discretization of the source term can improve the behaviour of the numerical scheme. In viscoelastic flows the convective terms are too small in comparison with the source terms and special treatment of the source term is necessary. The source terms for the x-momentum equation (Eq. (31)) can be written as

$$S_x = \underbrace{\frac{\partial \tau'_{xx}}{\partial x}}_{S_{x1}} + \underbrace{\frac{\partial \tau'_{xy}}{\partial y}}_{S_{x2}} + \underbrace{\mu \frac{\partial}{\partial x}\left(\frac{\partial u}{\partial x} + \frac{\partial v}{\partial y}\right)}_{S_{x3}}, \tag{33}$$

and for the y-momentum equation (Eq. (32)), the source term can be written as

$$S_y = \underbrace{\frac{\partial \tau'_{yy}}{\partial y}}_{S_{y1}} + \underbrace{\frac{\partial \tau'_{xy}}{\partial x}}_{S_{y2}} + \underbrace{\mu \frac{\partial}{\partial y}\left(\frac{\partial u}{\partial x} + \frac{\partial v}{\partial y}\right)}_{S_{y3}}. \tag{34}$$

The calculation of term S_{x1} requires the calculation of the first gradient of τ'_{xx}. The gradient of τ'_{xx} can be calculated using two approaches:

(1) Calculate the first derivative of velocity in x-direction and calculate the values of τ'_{xx} in the entire computational domain. After that, calculate the gradients at the nodes by interpolating the values of τ'_{xx} on the faces between two adjacent nodes.

(2) Substitute Eq. (28) in terms of S_{x1} giving $(\partial \tau'_{xx})/(\partial x) = (\partial \tau_{xx})/(\partial x) - 2\mu(\partial^2 u)/(\partial x^2)$ and thus avoid the calculation of the first derivative of velocities.

In this paper the second approach has been used. The advantage in this calculation of the second derivative is that the values at the node the derivative is referred to and the values at the two adjacent nodes are participating in its calculation. On the contrary, for the first derivative calculation only the values at the adjacent nodes participate [13]. A full explanation of the discretization of terms S_{x1}, S_{x2}, S_{y1}, S_{y2} is given in Appendix B.

The terms S_{x3} and S_{y3} are equal to zero when the continuity equation is satisfied. When they are set to zero from the early steps of the iterative procedure, the algorithm is harder to converge. The role of these terms is to stabilise the solution procedure without affecting the final solution as they tend to zero when convergence is approached. This stabilising effect can be enhanced if the relaxation technique introduced by these terms is increased. The enhancement is performed by multiplying them with a constant U_L.

This relaxation technique can be viewed as a specialized preconditioning of the matrix derived from the discretized equations. Actually the enhancement of terms S_{x3} and S_{y3} through the linearized source treatment results in the addition of a term on the left-hand side of Eq. (21) for the current iteration, while on the right-hand side the same term from the previous iteration is added. This really amounts to an under-relaxation procedure. Since U_L is really an under-relaxation factor for highly non-linear problems, it is problem-specific, i.e. it depends on the nature of the problem solved, the number of grid points, the grid spacing, the iterative procedure and the De number.

The factor U_L should be increased when the fluid elasticity becomes higher. During numerical trials, it was found that a low value of U_L resulted in divergence, while a high value resulted in slow convergence of the numerical scheme. In the present simulations, U_L was found to exhibit almost an exponential relationship with fluid elasticity, namely the Deborah number. The appropriate choice of U_L was found by starting from $U_L = 4$ for $De \leq 1.2$. From the experience gained from trial runs and knowing its exponential behaviour with De number, the next value of U_L was guessed for the higher De number computation. More details about this kind of relationship for the problem at hand is presented in the results and discussion section.

Using this new method of handling the source term by introducing the U_L factor, the well-known phenomenon of losing convergence with grid refinement [16] for high Deborah numbers was overcome.

3.4. Discretization of boundary conditions at the wall

The computation of the Neumann boundary conditions along the wall affects dramatically the solution accuracy. As the first gradients of all primitive variables are dominant in the source terms of the conservation equations, a second-order accuracy for the primitive variables is necessary. In this context quadratic polynomials [27] are used to describe the velocity variations along the wall (Appendix C). Using this formulation the maximum error was reduced approximately by 10 orders of magnitude compared with results obtained by considering the velocity as a linear function of displacement.

3.5. Solution of the discretized equations

In non-linear problems the equations are solved with iterative methods using an initial guess for the primitive variables and giving an approximate solution. The iterative methods have the advantage of minimum requirements regarding computer memory as they take advantage of zero elements in the coefficient matrix. In this work, the strongly implicit procedure (SIP) [28] is used. The SIP solution algorithm involves the direct, simultaneous solution of the set of equations formed by modification of the original matrix equation. The modified matrix is constructed according to two criteria: (a) the equation set must remain more strongly implicit than in the alternating direction implicit (ADI) case; and (b) the elimination procedure for the modified set must be economically efficient. These issues are addressed in detail in [29].

4. Results and discussion

The results were obtained using the code FIVOS developed in the Department of Chemical Engineering at NTUA [30]. The code is adapted to handle viscoelasticity according to the algorithm explained in the previous sections.

To establish confidence in the new FVM scheme implemented in this work, the solution of the one-directional Poiseuille flow of a UCM fluid model between two flat plates was first tested. This problem has an exact solution and has been extensively used as a test for various numerical schemes. The agreement between the analytical and the FVM solutions was excellent even for Deborah numbers up to 10^9. Also the experiments by Back and Roschke [31] have been successfully simulated for the case of the abrupt circular channel expansion of a Newtonian fluid certifying the consistency of the method for cases with changes in geometry.

4.1. Numerical simulation of the UCM model through a sudden expansion

In this section the simulations for the UCM model earlier undertaken by Darwish et al. [16] are repeated and extended for higher Deborah numbers and denser grids using the same differential constitutive equation.

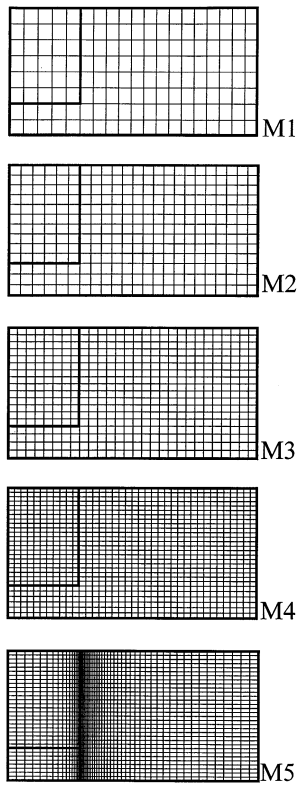

Fig. 4. The five grids used in the calculation of the 4:1 sudden expansion problem. Note that M1 and M2 resemble the grids used in the previous work by Darwish et al. [16].

As shown in Fig. 1, we consider flow through a sudden 4:1 planar expansion. The dimensionless Deborah number (De) defined previously has been used as the kinematic parameter controlling both the flow kinematics and, through the constitutive equation, the flow dynamics. The values of De are in the range between 0 and 3.0 ($0 \leq \mathrm{We} \leq 3$ according to [16]), while the Re number was set equal to 0.1 for all simulations as done in the previous work by Darwish et al. [16].

Table 2
Details of the grids used. Each node has six degrees of freedom

Grid	Number of cells	Number of unknowns[1]	Size of smallest cell near expansion corner	
			$\Delta x/H$	$\Delta y/H$
M1	210	864	0.400	0.250
M2	375	1746	0.333	0.167
M3	600	2976	0.250	0.125
M4	1200	6336	0.182	0.083
M5	1972	10 752	0.063	0.031

[1] The number of unknowns is the number of degrees of freedom minus the number of boundary conditions.

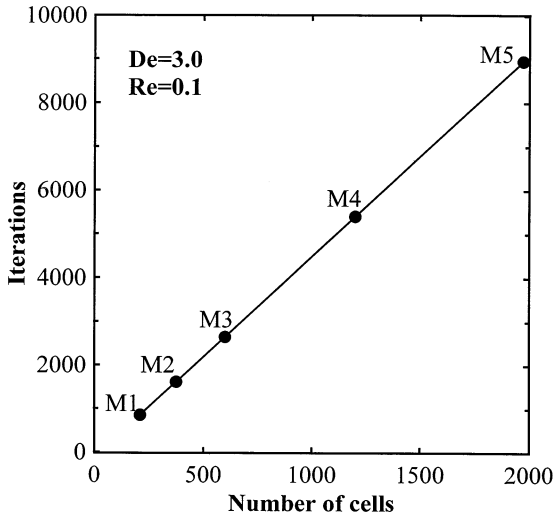

Fig. 5. Number of iterations versus grid density for De = 3.0 and Re = 0.1 to achieve a tolerance of 5×10^{-4} for the residuals of all variables. Note the linear convergence behaviour of the finite volume method.

For the finite volume discretization five grids have been used (Fig. 4 and Table 2). Due to the non-staggered grid geometry, for each grid the number of cells is equal to the number of nodes. The first one (M1) had 210 cells, giving a total of 864 unknowns. The second grid (M2) was more dense, having 375 cells, giving a total of 1746 unknowns. Similar grids to M1 and M2 were used by Darwish et al. [16] as the most dense grids for their simulations. A third grid (M3) having 600 cells and 2976 unknowns was also used to gain experience on the fluid behaviour through the expansion. To check the mesh dependency of the solution, a fourth grid (M4) having 1200 cells and 6336 unknowns was used. The workhorse of the present simulations was grid M5, having 1972 cells and 10752 unknowns.

The solution of a Newtonian fluid was obtained first, which in turn was used as an initial guess for the subsequent simulations with the viscoelastic model. At a given flow rate (or equivalently, Deborah number De), a converged solution was considered to have been reached for the non-linear set of equations when the value of all residuals was less than 5×10^{-4}. In Fig. 5, the number of total iterations needed are presented for several grids and De = 3.0. The iterations, or equivalently the computational time, exhibit a linear dependence with grid density. The execution times needed to achieve a maximum residual 5×10^{-4} for all primitive variables

Table 3
Total CPU time in seconds for computations on a PC equipped with a Pentium processor at 100 MHz

Grid	De	Re	Iterations	Total CPU time (s)
M1	0.8	0.1	209	25
M1	1.2	0.1	223	27
M5	3.0	0.1	9000	9028

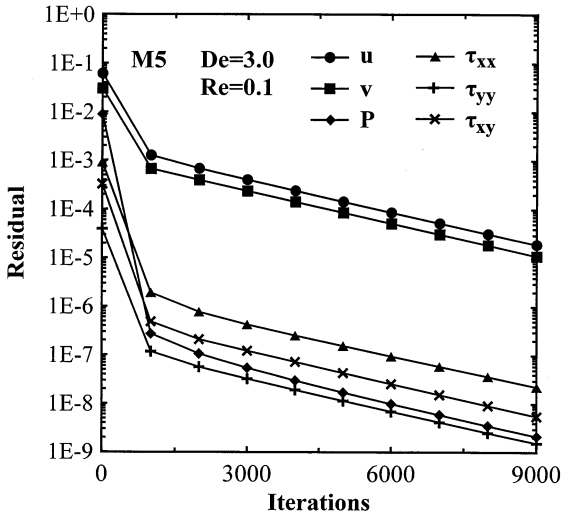

Fig. 6. Residual versus number of iterations for De = 3.0 and Re = 0.1 with grid M5 for all the solution variables.

are presented in Table 3 for runs made on a personal computer (PC) with a Pentium processor running at 100 MHz. According to Table 3, the total CPU time to reproduce the results by Darwish et al. [16] is equal to 27 s, while to achieve a grid-independent solution for De = 3.0 (starting from De = 0) the time consumed was equal to 9028 s (i.e. 2.5 h).

Fig. 6 shows the residuals for all primitive variables with the number of iterations for runs made at the highest De number and grid M5. The solution process required 9000 iterations. Fig. 7 shows the behaviour of the dimensionless pressure along the centerline of the expansion for the highest De = 3.0. Grid-independent results are obtained for grids more dense than M3.

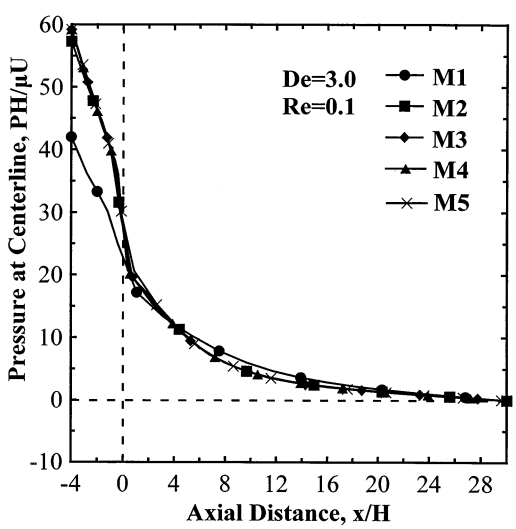

Fig. 7. Dimensionless axial pressure distribution along the centerline for flow of a UCM fluid in a 4:1 sudden expansion for different grids (De = 3.0, Re = 0.1).

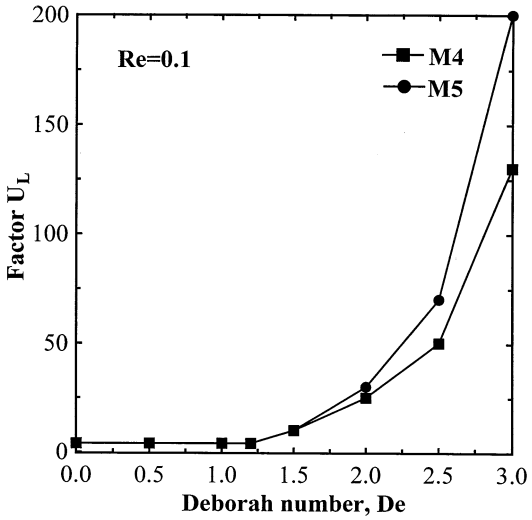

Fig. 8. Values of the U_L factor as a function of Deborah number for grids M4 and M5. Note the exponential increase as De increases.

Fig. 8 shows the values of the U_L factor as a function of Deborah number for grids M4 and M5. It is noticed that when U_L increases the stability increases, however, more computational time is needed. For every De there is a minimum value of U_L to obtain a converged solution with minimum computational cost. Since U_L is an under-relaxation factor, its value is empirical and was found by experience on trial computations. It was noted that it increases exponentially, as shown in Fig. 8. This behaviour helped in guessing the next value for computations at higher De numbers. For high De the value of U_L gets higher, e.g. for the finest grid M5 the value of U_L for $De = 1.2$ is equal to 4, while for $De = 3.0$, U_L equals 200. This exponential behaviour of U_L and the corresponding increase in computational time for the specific problem of flow through a 4:1 expansion became more evident for $De > 3.0$ (simulations have been actually carried up to $De = 4.0$) and it was one of the reasons for presenting results from computations up to $De = 3.0$ (the others being the total lack of recirculation in the reservoir, the uninteresting velocity field and the need for a very long computational domain). The reasons for the difficulty to achieve a solution in the Maxwell calculations at high De values and its connection to the specific geometry (planar versus axisymmetric, contraction versus expansion, flow around a sphere versus cylinder, etc.) is still an open subject for study. It is, however, clear that it is associated with extremely high normal stress values, which seem unrealistic to be sustained by any real fluid.

The Newtonian case ($De = 0.0$) in the planar expansion geometry was studied to verify the consistency of the method for two-dimensional problems. Fig. 9a shows the streamlines normalized between the values of 1 at the centerline and 0 at the walls, with increments of 0.1 in between. Recirculation zones are formed in the reservoir of the expansion as is well-known, with 0.19% of the flow rate rotating in a vortex envelope. Fig. 9b shows 20 evenly spaced isobars between the maximum and minimum values made dimensionless with the mean stress ($\mu U/H$). The overall pressure drop of 14.4 (dimensionless entrance correction $n_{en} = 0.34$) and the

dimensionless vortex length (0.15) are in very good agreement with previous results [2]. Fig. 9c–e show 20 evenly spaced contours for the normal and shear stresses between the maximum and minimum values made again dimensionless with the mean stress.

The viscoelastic simulations have been pursued first under exactly the same conditions as in the previous work by Darwish et al. [16] for direct comparison. The reservoir length L_{res} was set at $10H$. Fig. 10a shows the streamlines for $De = 1.2$ (or $We = 1.2$ according to [16]) and

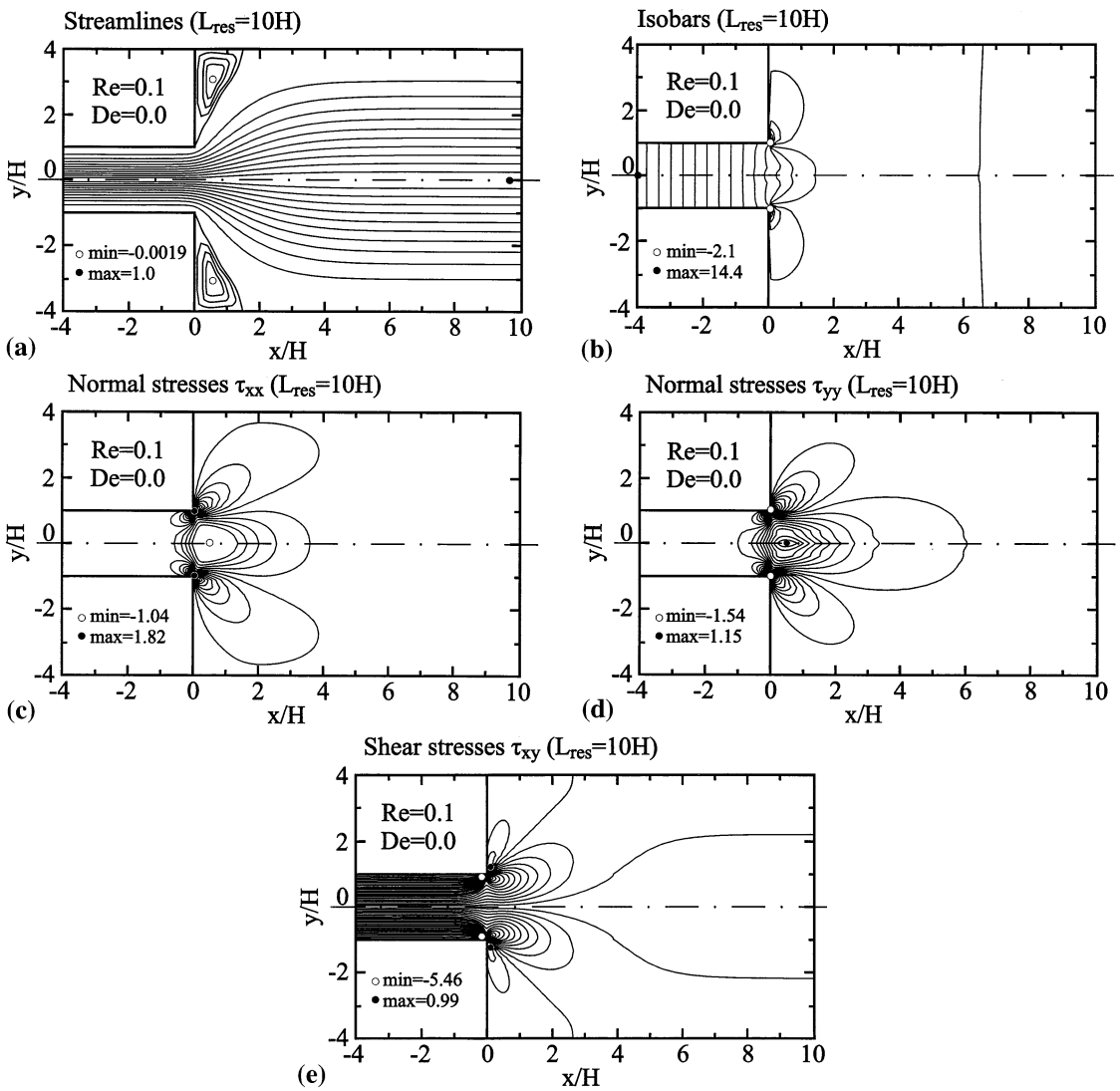

Fig. 9. Field contours for the flow of a Newtonian fluid in a 4:1 sudden expansion ($De = 0$, $Re = 0.1$) obtained with grid M5: (a) streamlines; (b) isobars; (c) τ_{xx} stress contours; (d) τ_{yy} stress contours; and (e) τ_{xy} stress contours. The contour values are equally spaced between the maximum and minimum values given on the graphs. Ten contours are drawn for the streamlines and 20 contours for pressure and stresses.

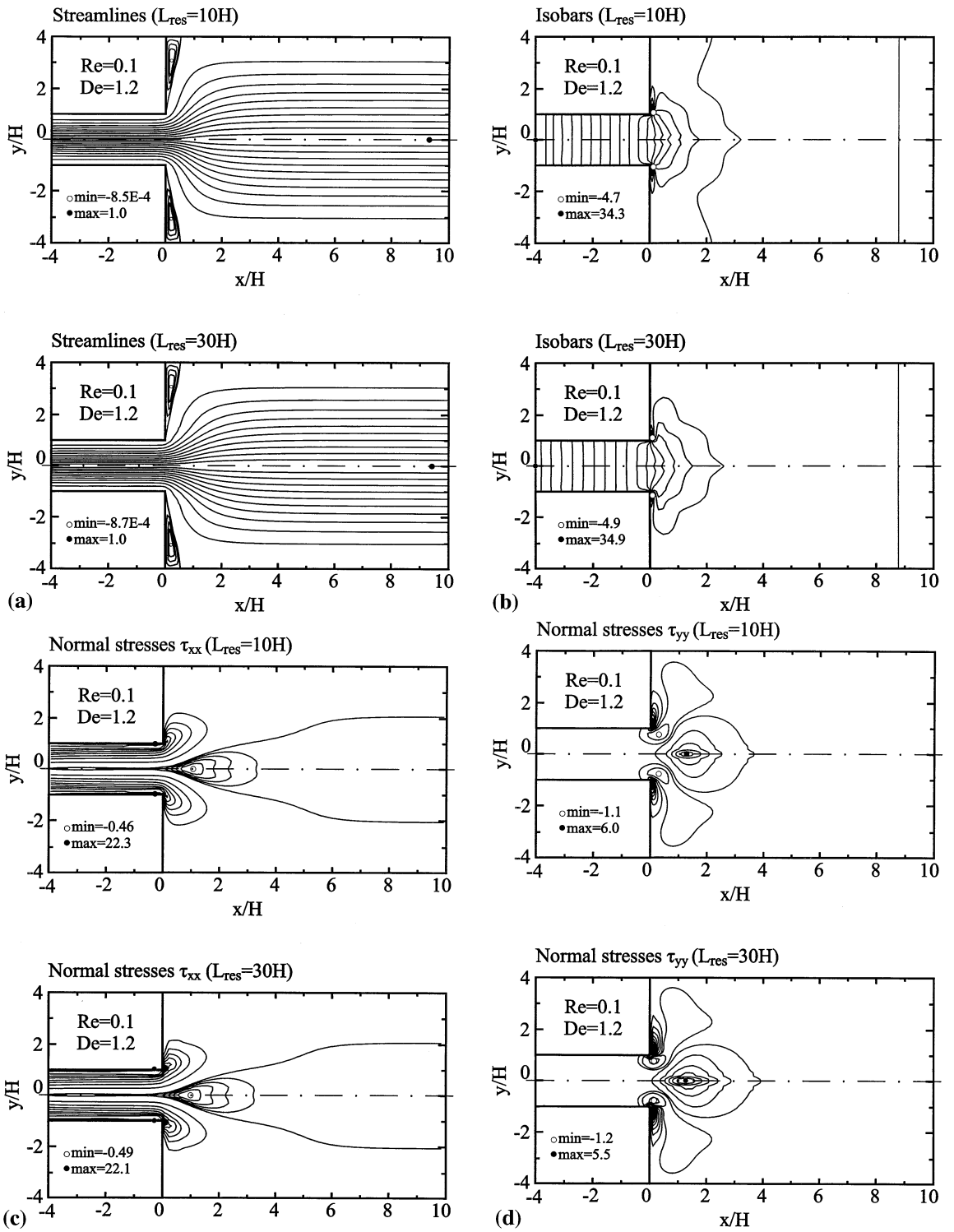

Fig. 10. Field contours for the flow of a UCM fluid in a 4:1 sudden expansion (De = 1.2, Re = 0.1) obtained with grid M5: (a) streamlines; (b) isobars; (c) τ_{xx} stress contours; (d) τ_{yy} stress contours; and (e) τ_{xy} stress contours. The contour values are equally spaced between the maximum and minimum values given on the graphs. Ten contours are drawn for the streamlines and 20 contours for pressure and stresses.

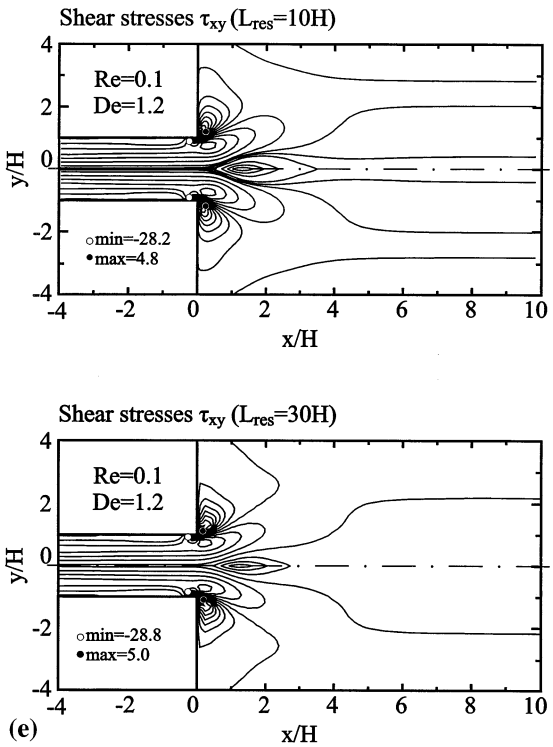

Fig. 10. (*Continued*)

$\mathrm{Re} = 0.1$, for which there are complete results for all variables from the previous viscoelastic computations for this problem. It is noted that viscoelasticity results in reducing the extent and intensity of the recirculation zones in the reservoir corners of the sudden expansion. The reason is that when the fluid is entering a channel of larger height, it will try to relax its stresses along the streamlines. For incompressible viscoelastic fluids this causes expansion in the transverse flow direction [32]. This behaviour is opposite to what occurs in a contraction geometry, where the fluid relaxes its stresses by increasing the recirculation zones.

Fig. 10b shows the isobars for $\mathrm{De} = 1.2$ and $\mathrm{Re} = 0.1$. The increase in relaxation time (or elasticity level) results in an increased pressure drop through the expansion with respect to the Newtonian result. Fig. 10c shows the contours for the normal stresses τ_{xx}. The viscoelasticity of the fluid is manifested by the appearance of large normal stresses along the inlet channel that stretch out into the reservoir in contrast with the Newtonian case (Fig. 10c). Fig. 10d shows contours of the normal stresses τ_{yy}, while Fig. 10e shows the corresponding contours for the shear stresses τ_{xy}.

As mentioned above, this viscoelastic case ($\mathrm{De} = 1.2$, $\mathrm{Re} = 0.1$) has been studied earlier by Darwish et al. [16], who present similar results for the streamlines, isobars and stress contours. When compared to previous solutions [16], the present solutions are smoother and physically more realistic (i.e. the pressure contours along the inlet channel are normal to the wall and the shear stress contours are parallel to the wall).

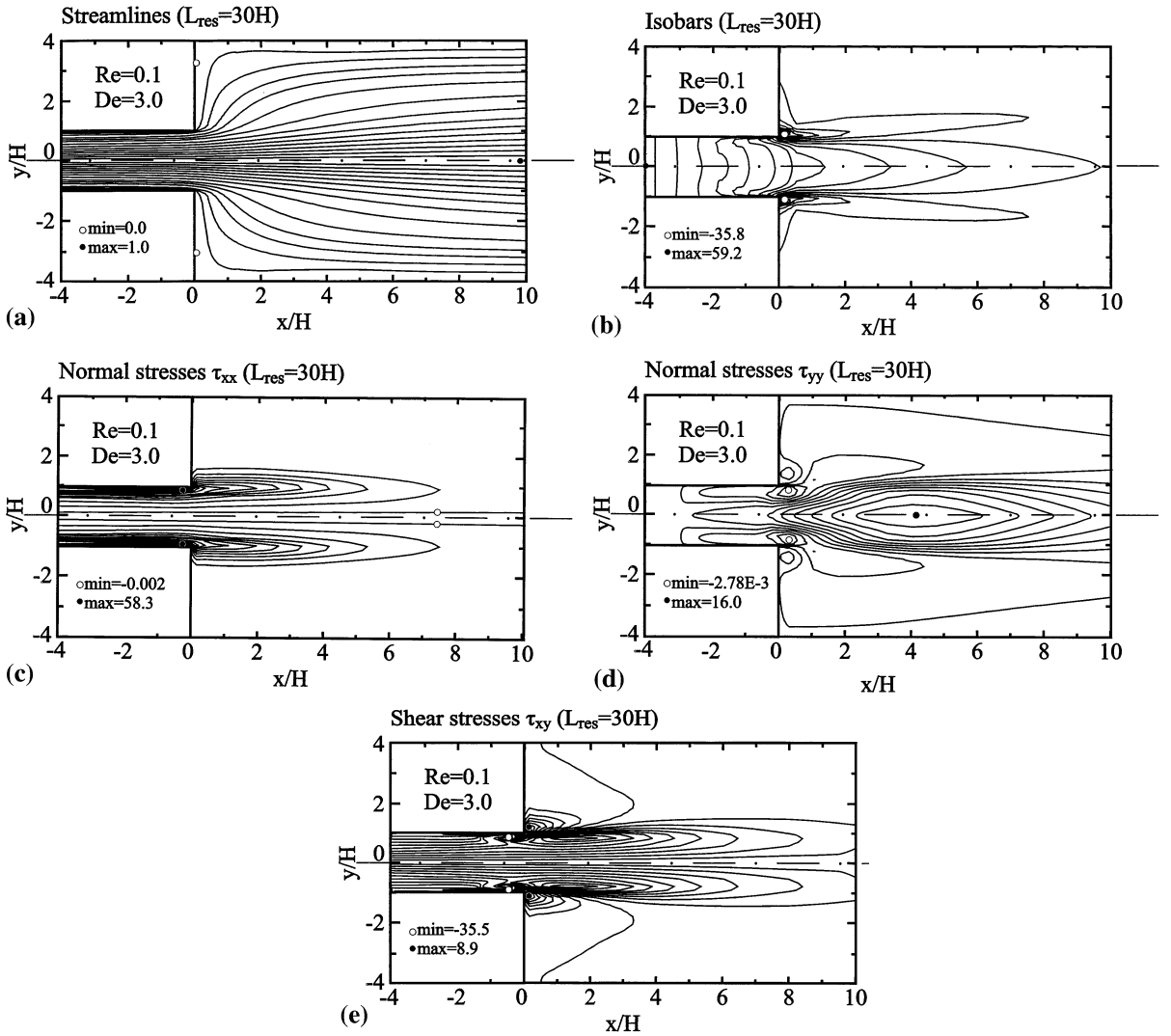

Fig. 11. Field contours for the flow of a UCM fluid in a 4:1 sudden expansion (De = 3.0, Re = 0.1) obtained with grid M5: (a) streamlines; (b) isobars; (c) τ_{xx} stress contours; (d) τ_{yy} stress contours; and (e) τ_{xy} stress contours. The contour values are equally spaced between the maximum and minimum values given on the graphs. Ten contours are drawn for the streamlines and 20 contours for pressure and stresses.

A further increase in the De number showed that the convergence was still good, but that physically unrealistic values were obtained for the field variables due to a short reservoir having a length of $L_{\text{res}} = 10H$. We believe this is the reason why the results by Darwish et al. [16] for We = 2.4 and Re = 0.1 are not physically correct for the pressures and the streamlines and they are not shown for the stresses. A severe bending of the streamlines will occur when a short domain is used to impose fully-developed velocity profiles at the inlet and/or outlet. Thus, it became obvious that a longer domain was necessary in order for the stresses to relax for higher

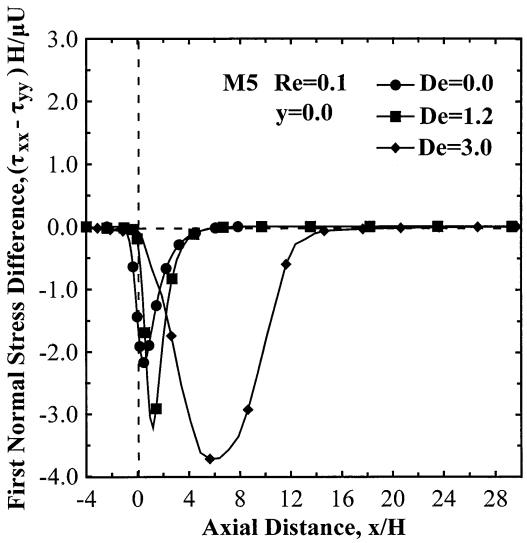

Fig. 12. Dimensionless first normal stress difference (N_1) distribution along the centerline for flow of a UCM fluid in a 4:1 sudden expansion for different De numbers (Re = 0.1, grid M5).

elasticity levels. A reservoir length of $30H$ was then assumed and the simulations were repeated for grid M5. The runs at De = 1.2 and Re = 0.1 showed that for this case a length of $10H$ was adequate, since the results did not differ appreciably by having reservoir lengths of either $10H$ or $30H$.

Further increasing the De number resulted in a further suppression and finally in a total elimination of the recirculation zones in the reservoir as shown in Fig. 11a, where the

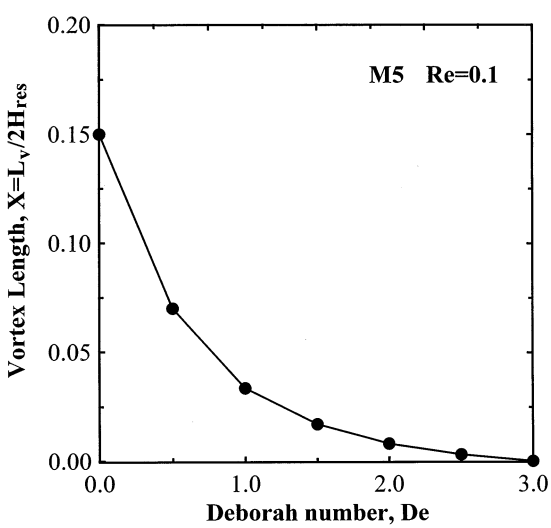

Fig. 13. Dimensionless vortex length versus Deborah number for flow of a UCM fluid in a 4:1 sudden expansion (Re = 0.1, grid M5).

streamlines are presented for $De = 3.0$ and $Re = 0.1$. A bending of the streamlines is noticed towards the walls as the fluid enters the sudden expansion. The pressure contours (Fig. 11b) along the channel are vertical only at the inlet and they are stretched deeply into the expansion reservoir. The maxima and minima are also much higher. The same type of behaviour is observed for the normal and shear stresses as presented in Fig. 11c–e. This happens because the elastic behaviour of the fluid is much stronger than the viscous one.

The values of normal stresses provide useful information on the fluid behaviour in processing and their first difference $N_1 = \tau_{xx} - \tau_{yy}$ can be measured experimentally. Fig. 12 provides the distribution of the dimensionless first normal stress difference N_1 along the centerline for three values of the Deborah number. It is seen that it is zero in the inlet channel, goes through a high increase after the entry in the expansion and then returns to zero farther and farther away as the elasticity level increases. This figure also shows how the maxima get transported down the channel and that a sufficiently long domain is necessary for the stresses to fully relax back to zero.

Another feature of the problem at hand is the dimensionless vortex length X defined as [1,2]

$$X = \frac{L_v}{2H_{res}}, \tag{35}$$

where L_v is the length of the vortex and $2H_{res}$ is the reservoir height (Fig. 1). Fig. 13 presents X as a function of Deborah number. The dimensionless vortex length becomes reduced from its Newtonian value of 0.15 down to 0.0 at $De = 3.0$. It is thus established that viscoelasticity reduces and finally eliminates the small Newtonian vortex in expansions for creeping flows (small Re numbers).

5. Concluding remarks

In this paper, the flow of a UCM model fluid through a 4:1 sudden planar expansion has been studied using a stable finite volume scheme. The choice of the problem was due to its earlier study by another research group [16] by the same method, thus allowing a direct comparison. The solution method succeeds in obtaining accurate values for all variables (including the stresses) at elasticity levels up to $De = 3.0$ with a variety of grids to establish results independent of grid density.

Using the FVM, correctly balanced forces over each control volume are obtained. As a result, the stresses near the singularity yield finite forces on the corner boundary. In addition, the non-staggered grid, where the same set of control volumes is used for all primitive variables, offers great geometrical simplicity, especially for posing the boundary conditions near the singularity. To enhance the accuracy of the method, the boundary conditions were imposed via quadratic polynomials. Accurate calculation of the primitive variables yielded accurate calculation of their first gradients, which are dominant in the source terms of the momentum equations. The numerical stability of the method depended on the order of precision in the calculation of source terms.

The conservation equations of stresses were transformed using the elastic–viscous split method introduced by Perera and Walters [7]. The convective terms for the stresses were

computed using a first-order upwind scheme, while for the velocities a hybrid scheme was used. A new method to discretize the source term of the momentum equations was introduced and the obstacle of flow type change occurring at high De was overcome. For low De and grid density, the solution was compared against other numerical results available in the literature [16] and found to give smoother and physically more correct results. For high De values ($De > 2.0$), it was found necessary to extend the domain appreciably in order to give enough length for the high viscoelastic stresses to relax. For $De > 3.0$, it was found that the stresses become exceedingly high, thus requiring a much longer domain, severe under-relaxation and a very high computational time, while the velocity field remained uninteresting (lack of recirculation).

The present simulations reinforce the point made previously by the Phan-Thien/Tanner group that the FVM can be used as a viable alternative for the solution of viscoelastic problems. The results are accurate and offer an improvement over previous numerical solutions. Although the present study has been applied to a UCM fluid in a relatively simple geometry, it can be further extended to other more realistic constitutive equations, such as the Phan-Thien/Tanner or Giesekus–Leonov models, etc. and to other geometries encountered in polymer processing.

Acknowledgements

Financial assistance from the Natural Sciences and Engineering Research Council (NSERC) of Canada and the Ontario Center for Materials Research (OCMR) for Professor E. Mitsoulis is gratefully acknowledged.

Appendix A. Momentum interpolation

The momentum interpolation technique is used to avoid uniform pressure field in a non-staggered grid. From the momentum equations (Eqs. (10) and (11)) and referring to Fig. 3, when solving for the velocity u_P and subtracting from the source term the part which contains the pressure, i.e. $b = b_P - A_P(P_e - P_w)$, we obtain[1]

$$u_P = \frac{\sum \alpha^u_{nbP} u_{nbP}}{\alpha^u_P} + \frac{b^u_P}{\alpha^u_P} - \frac{A^x_P}{\alpha^u_P}(P_e - P_w) \tag{A1}$$

Similarly for the velocity u_E:

$$u_E = \frac{\sum \alpha^u_{nbE} u_{nbE}}{\alpha^u_E} + \frac{b^u_E}{\alpha^u_E} - \frac{A^x_E}{\alpha^u_E}(P_{ee} - P_e) \tag{A2}$$

The velocity at the east surface of the cell with P as its center is:

[1] The exponents represent the primitive variable.

$$u_e = \frac{\sum \alpha^u_{nbe} u_{nbe}}{\alpha^u_e} + \frac{b^u_e}{\alpha^u_e} - \frac{A^x_e}{\alpha^u_e}(P_E - P_P) \tag{A3}$$

The unknown terms in Eq. (A3) are computed by linear interpolation of Eqs. (A1) and (A2) as follows:

$$\frac{\sum \alpha^u_{nbe} u_{nbe}}{\alpha^u_e} + \frac{b^u_e}{\alpha^u_e} = f^x_P \left(\frac{\sum \alpha^u_{nbE} u_{nbE}}{\alpha^u_E} + \frac{b^u_E}{\alpha^u_E} \right) + (1 - f^x_P) \left(\frac{\sum \alpha^u_{nbP} u_{nbP}}{\alpha^u_P} + \frac{b^u_P}{\alpha^u_P} \right) \tag{A4}$$

$$\frac{1}{\alpha^u_e} = f^x_P \frac{1}{\alpha^u_E} + (1 - f^x_P) \frac{1}{\alpha^u_P} \tag{A5}$$

Substituting Eq. (A4) in Eq. (A3) yields:

$$u_e = f^x_P \left(\frac{\sum \alpha^u_{nbE} u_{nbE}}{\alpha^u_E} + \frac{b^u_E}{\alpha^u_E} \right) + (1 - f^x_P) \left(\frac{\sum \alpha^u_{nbP} u_{nbP}}{\alpha^u_P} + \frac{b^u_P}{\alpha^u_P} \right) - \frac{A^x_e}{\alpha^u_e}(P_E - P_P) \tag{A6}$$

and substituting the term $((\Sigma\, \alpha^u_{nbE} u_{nbE})/(\alpha^u_E)) + (b^u_E/\alpha^u_E)$ from Eq. (A2) and the term $((\Sigma\, \alpha^u_{nbP} u_{nbP})/(\alpha^u_P)) + (b^u_P/\alpha^u_P)$ from Eq. (A1), Eq. (A6) takes the form:

$$u_e = f^x_P u_E + (1 - f^x_P) u_P + f^x_P \frac{A^u_E}{\alpha^u_E}(P_{ee} - P_e) + (1 - f^x_P) \frac{A^u_P}{\alpha^u_P}(P_e - P_w) - \frac{A^x_e}{\alpha^u_e}(P_E - P_P) \tag{A7}$$

Setting:

$$u_{me} = f^x_P u_E + (1 - f^x_P) u_P \tag{A8}$$

and

$$u_{ce} = f^x_P \frac{A^u_E}{\alpha^u_E}(P_{ee} - P_e) + (1 - f^x_P) \frac{A^u_P}{\alpha^u_P}(P_e - P_w) - \frac{A^x_e}{\alpha^u_e}(P_E - P_P) \tag{A9}$$

Eq. (A7) can be written:

$$u_e = u_{me} + u_{ce} \tag{A10}$$

where u_{me} is the velocity derived from the linear interpolation of velocities u_P and u_E at point e and u_{ce} is the velocity derived from the momentum interpolation at point e.

Appendix B. Discretization of the source term

The source terms of the momentum equations (Eqs. (33) and (34)) include the terms S_{x1} and S_{x2}. The term S_{x1} is calculated as:

$$S_{x1} = \frac{\partial \tau'_{xx}}{\partial x} = \frac{\partial \tau_{xx}}{\partial x} - 2\mu \frac{\partial^2 u}{\partial x^2} \tag{B1}$$

The term $\partial\tau_{xx}/\partial x$ is added in the source assuming quadratic variation of τ_{xx} along the x-direction. Thus, $\partial\tau_{xx}/\partial x$ is written as $(2\alpha_1 x+\beta_1)\,\Delta x\,\Delta y$. For the calculation of α_1 and β_1, the same practice as that described in Appendix C was used, giving:

$$\beta_1=\frac{\tau_{xx_P}-\tau'_{xx_W}}{x_P-x_W}-\alpha_1(x_P+x_W) \tag{B2}$$

$$\alpha_1=\frac{\dfrac{\tau_{xx_E}-\tau_{xx_W}}{x_E-x_W}-\dfrac{\tau_{xx_P}-\tau_{xx_W}}{x_P-\tau_{xx_W}}}{x_E-x_P} \tag{B3}$$

The term $-2\mu((\partial^2 u)/(\partial x^2))$ is calculated by integrating it over the control volume V:

$$\int_{V_P}-2\mu\frac{\partial^2 u}{\partial x^2}\,\mathrm{d}V=\int_{y_s}^{y_n}\int_{x_w}^{x_e}-2\mu\frac{\partial^2 u}{\partial x^2}\,\mathrm{d}x\,\mathrm{d}y=-2D_e(u_E-u_P)+2D_w(u_P-u_w) \tag{B4}$$

Consequently:

$$S_{x1}=(2\alpha x+\beta)\,\Delta x\,\Delta y-2D_e(u_E-u_P)+2D_w(u_P-u_w) \tag{B5}$$

The term S_{x2} is calculated as:

$$S_{x2}=\frac{\partial\tau'_{xy}}{\partial y}=\frac{\partial\tau_{xy}}{\partial y}-\mu\frac{\partial}{\partial y}\left(\frac{\partial u}{\partial y}+\frac{\partial v}{\partial x}\right) \tag{B6}$$

The term $\partial\tau_{xy}/\partial y$ is calculated following the same method as in term S_{x1}. The term $-\mu(\partial/\partial y)((\partial u/\partial y)+(\partial v/\partial x))$ is calculated by integrating it over the control volume V:

$$\begin{aligned}\int_{V_P}-\mu\frac{\partial}{\partial y}\left(\frac{\partial u}{\partial y}+\frac{\partial v}{\partial x}\right)\mathrm{d}V&=\int_{y_s}^{y_n}\int_{x_w}^{x_e}-\mu\left(\frac{\partial^2 u}{\partial y^2}+\frac{\partial^2 v}{\partial y\partial x}\right)\mathrm{d}x\,\mathrm{d}y\\&=-D_n(u_N-u_P)+D_s(u_P-u_S)-\mu(v_{ne}-v_{nw}-v_{se}+v_{sw})\end{aligned} \tag{B7}$$

Consequently:

$$S_{x2}=(2\alpha_2 y+\beta_2)\,\Delta x\,\Delta y-D_n(u_N-u_P)+D_s(u_P-u_S)-\mu(v_{ne}-v_{nw}-v_{se}+v_{sw}) \tag{B8}$$

where:

$$\beta_2=\frac{\tau_{xy_P}-\tau_{xy_S}}{y_P-y_S}-\alpha_2(y_P+y_S) \tag{B9}$$

$$\alpha_2=\frac{\dfrac{\tau_{xy_N}-\tau_{xy_S}}{y_N-y_S}-\dfrac{\tau_{xy_P}-\tau_{xy_S}}{y_P-y_S}}{y_N-y_P} \tag{B10}$$

The term S_{y1} is calculated as:

$$S_{y1}=\frac{\partial\tau'_{yy}}{\partial y}=\frac{\partial\tau_{yy}}{\partial y}-2\mu\frac{\partial^2 v}{\partial y^2} \tag{B11}$$

The term $\partial\tau_{yy}/\partial y$ is calculated following the same method as the derivative of stress in term S_{x1}. The term $-2\mu(\partial^2 v/\partial y^2)$ is calculated by integrating it over the control volume V:

$$\int_{V_P} -2\mu \frac{\partial^2 v}{\partial y^2}\,\mathrm{d}V = \int_{y_z}^{y_n}\int_{x_w}^{x_e} -2\mu \frac{\partial^2 v}{\partial y^2}\,\mathrm{d}x\,\mathrm{d}y = -2D_n(v_N - v_P) + 2D_s(v_P - v_S) \tag{B12}$$

Consequently:

$$S_{y1} = (2\alpha_3 y + \beta_3)\,\Delta x\,\Delta y - 2D_n(v_N - v_P) + 2D_s(v_P - v_S) \tag{B13}$$

where:

$$\beta_3 = \frac{\tau_{yy_P} - \tau_{yy_S}}{y_P - y_S} - \alpha_3(y_P + y_S) \tag{B14}$$

$$\alpha_3 = \frac{\dfrac{\tau_{yy_N} - \tau_{yy_S}}{y_N - y_S} - \dfrac{\tau_{yy_P} - \tau_{yy_S}}{y_P - y_S}}{y_N - y_P} \tag{B15}$$

The term S_{y2} is calculated as:

$$S_{y2} = \frac{\partial \tau'_{xy}}{\partial x} = \frac{\partial \tau_{xy}}{\partial x} - \mu \frac{\partial}{\partial x}\left(\frac{\partial u}{\partial y} + \frac{\partial v}{\partial x}\right) \tag{B16}$$

The term $\partial\tau_{xy}/\partial x$ is calculated following the same method as the derivative of stress in term S_{x1}. The term $-\mu(\partial/\partial x((\partial u/\partial y) + (\partial v/\partial x))$ is calculated by integrating it over the control volume V:

$$\int_{V_P} -\mu \frac{\partial}{\partial x}\left(\frac{\partial u}{\partial y} + \frac{\partial v}{\partial x}\right)\mathrm{d}V = \int_{y_s}^{y_n}\int_{x_w}^{x_e} -\mu \frac{\partial}{\partial x}\left(\frac{\partial u}{\partial y} + \frac{\partial v}{\partial x}\right)\mathrm{d}x\,\mathrm{d}y \tag{B17}$$

$$= -\mu(-u_{ne} + u_{se} - u_{nw} + u_{sw}) - D_e(v_E - v_P) + D_w(v_P - v_W) \tag{B18}$$

Consequently:

$$S_{y2} = (2\alpha_4 x + \beta_4)\,\Delta x\,\Delta y - \mu(-u_{ne} + u_{se} - u_{nw} + u_{sw}) - D_e(v_E - v_P) + D_w(v_P - v_W) \tag{B19}$$

where:

$$\beta_4 = \frac{\tau_{xy_P} - \tau_{xy_W}}{x_P - x_W} - \alpha_4(x_P + x_W) \tag{B20}$$

$$\alpha_4 = \frac{\dfrac{\tau_{xy_E} - \tau_{xy_W}}{x_E - x_W} - \dfrac{\tau_{xy_P} - \tau_{xy_W}}{x_P - x_W}}{x_E - x_P} \tag{B21}$$

The terms S_{x3} and S_{y3} are discretized as follows:

$$\int_{V_P} S_{x3}\,\mathrm{d}V = U_{\mathrm{L}} \int_{x_w}^{x_e}\int_{y_s}^{y_n} \mu \frac{\partial}{\partial x}\left(\frac{\partial u}{\partial x} + \frac{\partial v}{\partial y}\right)\mathrm{d}y\,\mathrm{d}x \tag{B22}$$

$$\int_{V_P} S_{y3}\,\mathrm{d}V = U_{\mathrm{L}} \int_{y_s}^{y_n}\int_{x_w}^{x_e} \mu \frac{\partial}{\partial y}\left(\frac{\partial u}{\partial x} + \frac{\partial v}{\partial y}\right)\mathrm{d}y\,\mathrm{d}x \tag{B23}$$

In the source term of the x-momentum equation the terms of Eq. (23) S_{x5} is included adding in S_C the term:

$$S_{C,x} = U_{\mathrm{L}}\left[\frac{\mu A_e}{(\delta x)_e}u_E + \frac{\mu A_w}{(\delta x)_w}u_W + \mu(v_{en} - v_{wn}) - \mu(v_{es} - v_{ws})\right] \tag{B24}$$

and in S_P:

$$S_{P,x} = -U_{\mathrm{L}}\left(\frac{\mu A_e}{(\delta x)_e} + \frac{\mu A_w}{(\delta x)_w}\right) \tag{B25}$$

while in the source term of the y-momentum equation the terms of Eq. (23) S_{y5} is included adding in S_C:

$$S_{C,y} = U_{\mathrm{L}}\left[\frac{\mu A_n}{(\delta y)_n}u_N + \frac{\mu A_s}{(\delta y)_s}u_s + \mu(u_{en} - u_{es}) - \mu(u_{wn} - u_{ws})\right] \tag{B26}$$

and in S_P:

$$S_{P,y} = -U_{\mathrm{L}}\left(\frac{\mu A_n}{(\delta y)_n} + \frac{\mu A_s}{(\delta y)_s}\right) \tag{B27}$$

Appendix C. Neumann boundary conditions

The discretization of velocity gradients on the wall boundaries affects dramatically the accuracy of the numerical method. A method to obtain second-order accuracy for the primitive variables is to use quadratic polynomials for posing the boundary conditions on the wall [27], adapted for a non-uniform grid.

The wall force is entered into the discretized u-momentum equation as a source. The wall shear stress value is obtained from

$$\tau_w = \mu\left.\frac{\partial u}{\partial y}\right|_P \tag{C1}$$

The shear force F_{s} is now given by:

$$F_{\mathrm{S}} = -\tau_w A \tag{C2}$$

where A is the wall area of the control volume.

The appropriate source term in the u-equation is defined by:

$$S = \mu A\left(\frac{\partial u}{\partial y}\right)\Bigg|_{\mathrm{wall}} \tag{C3}$$

The computation of the u-gradient in the y-direction in Eq. (C3) is carried out assuming that u is a quadratic function of y:

$$u = \alpha y^2 + \beta y + \gamma \tag{C4}$$

giving:

$$\frac{\partial u}{\partial y} = 2\alpha y + \beta \tag{C5}$$

Applying Eq. (C3) to grid points N, P and S, the following equations are derived:

$$u_N = \alpha y_N^2 + \beta y_N + \gamma \tag{C6}$$

$$u_P = \alpha y_P^2 + \beta y_P + \gamma \tag{C7}$$

$$u_S = \alpha y_S^2 + \beta y_S + \gamma \tag{C8}$$

In the above system of equations:

$$\beta = \frac{u_P - u_S}{y_P - y_S} - \alpha(y_P + y_S) \tag{C9}$$

$$\alpha = \frac{\dfrac{u_N - u_S}{y_N - y_S} - \dfrac{u_P - u_S}{y_P - y_S}}{y_N - y_P} \tag{C10}$$

Substituting Eq. (C5) in Eq. (C3) the following equation is valid:

$$S = \mu A(2\alpha y|_{\text{wall}} + \beta) \tag{C11}$$

Finally the source term is obtained by substituting the values of α and β in Eq. (C11):

$$S = \frac{\mu}{V}\left(2\frac{\dfrac{u_N - u_S}{y_N - y_S} - \dfrac{u_P - u_S}{y_P - y_S}}{y_N - y_P} y_N + \frac{u_P - u_S}{y_P - y_S} - \frac{\dfrac{u_N - u_S}{y_N - y_S} - \dfrac{u_P - u_S}{y_P - y_S}}{y_N - y_P}(y_P + y_S)\right)\Delta x \tag{C12}$$

References

[1] R. Keunings, Simulation of viscoelastic fluid flow, in: C.L. Tucker III (Ed.), Fundamentals of Computer Modelling for Polymer Processing, Carl Hanser Verlag, New York, 1989, pp. 403–469.

[2] E. Mitsoulis, Numerical simulation of viscoelastic fluids, in: N.P. Cheremisinoff (Ed.), Encyclopedia of Fluid Mechanics, vol. 9, Polymer Flow Engineering, Gulf Publishing Company, Dallas, Texas, USA, 1990, pp. 649–704.

[3] R.I. Tanner, From A to (BK)Z in constitutive equations, J. Rheol. 32 (1988) 673–702.

[4] H.P.W. Baaijens, G.W.M. Peters, F.P.T. Baaijens, H.E.H. Meijer, Viscoelastic flow past a confined cylinder of a polyisobutylene solution, J. Rheol. 39 (1995) 1243–1277.

[5] G. Barakos, E. Mitsoulis, Numerical simulation of viscoelastic flow around a cylinder using an integral constitutive equation, J. Rheol. 39 (1995) 1279–1292.

[6] M.J. Crochet, G. Pilate, Plane flow of a fluid of second grade through a contraction, J. Non-Newton. Fluid Mech. 1 (1976) 247–258.

[7] M.G.N. Perera, K. Walters, Long-range memory effects in flows involving abrupt changes in geometry. Part I. Flows associated with L-shaped and T-shaped geometries, J. Non-Newton. Fluid Mech. 2 (1977) 49–81.

[8] M.G.N. Perera, K. Walters, Long-range memory effects in flows involving abrupt changes in geometry. Part II. The expansion-contraction-expansion problem, J. Non-Newton. Fluid Mech. 2 (1977) 191–204.

[9] M.J. Crochet, A.R. Davies, K. Walters, Numerical Simulation of Non-Newtonian Flow, Elsevier, Amsterdam, 1984.

[10] M.B. Bush, J.F. Milthorpe, R.I. Tanner, Finite element and boundary element methods for extrusion computations, J. Non-Newton. Fluid Mech. 16 (1984) 37–51.

[11] M.B. Bush, R.I. Tanner, N. Phan-Thien, A boundary element investigation of extrudate swell, J. Non-Newton. Fluid Mech. 18 (1985) 143–162.

[12] A.N. Beris, R.C. Armstrong, R.A. Brown, Spectral/finite element calculations of the flow of a Maxwell fluid between eccentric rotating cylinders, J. Non-Newton. Fluid Mech. 22 (1987) 129–167.
[13] S.V. Patankar, Numerical Heat Transfer and Fluid Flow, Hemisphere, New York, 1980.
[14] H.H. Hu, D.D. Joseph, Numerical simulation of viscoelastic flow past a cylinder, J. Non-Newton. Fluid Mech. 37 (1990) 347–377.
[15] J.Y. Yoo, Y. Na, A numerical study of the planar contraction flow of a viscoelastic fluid using SIMPLER algorithm, J. Non-Newton. Fluid Mech. 39 (1991) 89–106.
[16] M.S. Darwish, J.R. Whiteman, M.J. Bevis, Numerical modelling of viscoelastic liquids using a finite-volume method, J. Non-Newton. Fluid Mech. 45 (1992) 311–337.
[17] G.P. Sasmal, A finite volume approach for calculation of viscoelastic flow through an abrupt axisymmetric contraction, J. Non-Newton. Fluid Mech. 47 (1995) 15–47.
[18] R.I. Tanner, N. Phan-Thien, X. Huang, Two and three-dimensional finite volume methods for flows of viscoelastic fluids, Proc. 4th Eur. Cong. Rheology, Seville, Spain, 1994, pp. 362–364.
[19] S.C. Xue, N. Phan-Thien, R.I. Tanner, Numerical study of secondary flows of viscoelastic fluid in straight pipes by an implicit finite volume method, J. Non-Newton. Fluid Mech. 59 (1995) 191–213.
[20] X. Huang, N. Phan-Thien, R.I. Tanner, Viscoelastic flow between eccentric rotating cylinders: unstructured control volume method, J. Non-Newton. Fluid Mech. 64 (1996) 71–92.
[21] X.-L. Luo, A control volume approach for integral viscoelastic models and its application to contraction flow of polymer melts, J. Non-Newton. Fluid Mech. 64 (1996) 173–189.
[22] R.I. Tanner, Engineering Rheology, Clarendon Press, Oxford, 1985.
[23] T.F. Miller, F.W. Schmidt, Use of a pressure weighted interpolation method for the solution of the incompressible Navier–Stokes equations on a non-staggered grid system, Numer. Heat Transf. 14 (1988) 213–233.
[24] S. Majumdar, Role of under-relaxation in momentum interpolation for calculation of flow with non-staggered grids, Numer. Heat Transf. 13 (1988) 125–132.
[25] J.P. Van Doormal, G.D. Raithby, Enhancement of the SIMPLE method for predicting incompressible flows, Numer. Heat Transf. 7 (1984) 147–163.
[26] C.R. Maliska, G.D. Raithby, Calculating 3D fluid flows using orthogonal grids, Proc. 3rd Int. Conf. Numerical Methods in Laminar and Turbulent Flows, Seattle, WA, 1986, pp. 656–666.
[27] D.A. Anderson, J.C. Tannehill, R.H. Pletcher, Computational Fluid Mechanics and Heat Transfer, McGraw-Hill, New York, 1984, pp. 57–61.
[28] C.A. Fletcher, Computational Techniques for Fluid Dynamics, vol. 2, 2nd ed., Springer, Berlin, 1991.
[29] A.S. Mujumdar, R.A. Mashelkar, Advances in Transport Processes, vol. 3, Wiley, Chichester, 1984.
[30] K. Missirlis, FIVOS: A FInite VOlume Solver for non-Newtonian flows, Internal Report, Department of Chemical Engineering, NTUA, Athens, Greece, 1996.
[31] L.H. Back, E.J. Roschke, Shear-layer flow regimes and wave instabilities and reattachment lengths downstream of an abrupt circular channel expansion, J. Appl. Mech. 9 (1972) 677–681.
[32] R.B. Bird, R.C. Armstrong, O. Hassager, Dynamics of Polymeric Liquids, vol. 1, Fluid Mechanics, Wiley, New York, 1977.